PNAS RESEARCH ARTICLE | PLANT BIOLOGY

Topoisomerase VI participates in an insulator-like function that prevents H3K9me2 spreading

Louis-Valentin Méteignier[a], Cécile Lecampion[a], Florent Velay[a], Cécile Vriet[a,b], Laura Dimnet[a], Martin Rougée[c,d], Christian Breuer[e], Ludivine Soubigou-Taconnat[f,g], Keiko Sugimoto[e], Fredy Barneche[c], and Christophe Laloi[a,1]

Edited by Steven Henikoff, Fred Hutchinson Cancer Research Center, Seattle, WA; received February 10, 2020; accepted April 19, 2022

The organization of the genome into transcriptionally active and inactive chromatin domains requires well-delineated chromatin boundaries and insulator functions in order to maintain the identity of adjacent genomic loci with antagonistic chromatin marks and functionality. In plants that lack known chromatin insulators, the mechanisms that prevent heterochromatin spreading into euchromatin remain to be identified. Here, we show that DNA Topoisomerase VI participates in a chromatin boundary function that safeguards the expression of genes in euchromatin islands within silenced heterochromatin regions. While some transposable elements are reactivated in mutants of the Topoisomerase VI complex, genes insulated in euchromatin islands within heterochromatic regions of the *Arabidopsis thaliana* genome are specifically down-regulated. H3K9me2 levels consistently increase at euchromatin island loci and decrease at some transposable element loci. We further show that Topoisomerase VI physically interacts with S-adenosylmethionine synthase methionine adenosyl transferase 3 (MAT3), which is required for H3K9me2. A Topoisomerase VI defect affects MAT3 occupancy on heterochromatic elements and its exclusion from euchromatic islands, thereby providing a possible mechanistic explanation to the essential role of Topoisomerase VI in the delimitation of chromatin domains.

euchromatin islands | heterochromatin spreading | insulator | topoisomerase VI | methionine adenosyltransferase

Significance

In the eukaryotic genome, DNA associates with proteins and forms two main types of chromatin, the highly condensed heterochromatin, which is inaccessible to transcription factors and hence transcriptionally silent, and the less condensed, hence transcriptionally active, euchromatin. The maintenance of sharp boundaries between these chromatin domains with antagonistic functionality is therefore critical for transcriptional control and involves chromatin insulators that remain unknown in plants. Here, we show that a plant topoisomerase participates in such a chromatin boundary function that prevents heterochromatin spreading into euchromatin, and hence safeguards the expression of genes in euchromatin islands within silenced heterochromatin regions. We have also identified partners of this topoisomerase that allow us to provide a mechanistic insight to this insulator-like function.

The discovery of position effect variegation in *Drosophila melanogaster* paved the way toward revealing the importance of chromatin contexts in the regulation of gene expression (1, 2). Since then, cytogenetic and molecular profiling of the epigenome, as well as topological analyses of chromatin architecture, have allowed the mechanisms involved in partitioning the gene-rich euchromatic fraction from the repeat-rich heterochromatic fraction to be elucidated. Large protein complexes specific to insulator DNA sequences contribute to partitioning chromatin domains with distinct identity at multiple scales. These complexes maintain the identity of adjacent genomic loci with antagonistic chromatin marks and functionality, and more globally influence the formation of long-range chromosomal interactions (3). Insulator binding proteins—such as the CCCTC-binding factor CTCF, BEAF-32, CP190, and Mod—have been best described in *Drosophila*, where they play critical roles in the definition of chromatin and transcriptional status. In vertebrates, CTCF is the only known insulator binding protein homolog. CTCF is enriched at insulator DNA sequences that define large topological domains of the genome (4–6) and, in some cases, define boundaries between adjacent chromatin domains with distinct features (7). Surprisingly, CTCF orthologs cannot be identified in many eukaryotic organisms, including plants (8). Moreover, very few studies support the presence of insulator DNA sequences or insulator-like regions in plants (9–11), and insulator binding factors remain to be identified.

This contrasts with the observation that *Arabidopsis thaliana* and other plant species display highly indexed chromatin states along the genome, with well-defined chromatin signatures around transcriptionally active or repressed genes, as well as close relationships between chromatin composition and genome topology in the nuclear space (12, 13). In *Arabidopsis*, heterochromatin is found on hundreds of transposable elements (TEs) mostly confined within the pericentromeric regions and at a few knob structures that tend to associate through long-distance interactions in the nuclear space (14–18). As a result, in *Arabidopsis* interphase nuclei most cytologically visible heterochromatin is condensed within 8 to 10 conspicuous foci that are referred to as chromocenters (19–21). Consistent with their heterochromatic nature, chromocenters are refractory to transcription and contain highly methylated DNA (22), as well as histone modifications, such as H3K9me2 and H3K27me2 (23, 24). Nonetheless, many expressed genes exhibiting euchromatic features appear to be located in close vicinity to large heterochromatic

Author contributions: L.-V.M., K.S., F.B., and C. Laloi designed research; L.-V.M., F.V., C.V., L.D., M.R., C.B., and C. Laloi performed research; C. Lecampion, L.S.-T., and K.S. contributed new reagents/analytic tools; L.-V.M., C. Lecampion, F.B., and C. Laloi analyzed data; and L.-V.M., F.B., and C. Laloi wrote the paper.

The authors declare no competing interest.

This article is a PNAS Direct Submission.

[1]To whom correspondence may be addressed. Email: christophe.laloi@univ-amu.fr.

This article contains supporting information online at http://www.pnas.org/lookup/suppl/doi:10.1073/pnas.2001290119/-/DCSupplemental.

Published June 27, 2022.

regions in the *Arabidopsis* genome, notably within the pericentromeric and knob regions (25, 26). The mechanisms by which gene-containing euchromatic islands (EIs) are insulated from neighboring heterochromatin regions and how their transcriptional capacities are preserved in such chromatin contexts are largely unknown. In this study, we have unveiled an essential function of the plant Topoisomerase VI (Topo VI) complex in preserving the functional and structural identity of EIs.

DNA topoisomerases are enzymes that introduce transient DNA breaks to resolve topological constraints that arise during multiple cellular processes, such as replication, transcription, recombination, and chromatin remodeling. The plant Topo VI, a type II topoisomerase first identified in the archaeon *Sulfolobus shibatae* (27, 28), was initially implicated in various biological processes involving endoreduplication, such as root hair growth (29–31), hypocotyl elongation (31), and nodule differentiation (32). Topo VI forms an A_2B_2 heterotetramer whose A and B subunits are encoded by single genes in *Arabidopsis*, *AtTOP6A*/*CAA39*/*AtSPO11-3*/*RHL2*/*BIN5*/*AT5G02820* and *AtTOP6B*/*RHL3*/*BIN3*/*HYP6*/*HLQ*/*AT3G20780*, respectively (33–37). Two additional subunits named ROOT HAIRLESS 1 (RHL1/HYP7/AT1G48380) and BRASSINOSTEROID-INSENSITIVE 4 (BIN4/MID/AT5G24630) (31, 38, 39) are essential for the *Arabidopsis* Topo VI function and appear to be evolutionarily conserved in plants and in other eukaryote groups, while their precise functions remain unclear. However, BIN4 shares sequence similarity with the C-terminal region of animal Topo IIα, which seems to have regulatory functions (40–42), and exhibits stable DNA binding in vitro (38). Therefore, it has been proposed that BIN4 may have a regulatory role in the plant Topo VI complex, presumably by holding the substrate DNA through its AT-hook motif (38, 39).

In recent years, evidence has accumulated that topoisomerases have more diverse and specialized functions than previously thought (43). In particular, transcriptomic analyses of several Topo VI mutants revealed that Topo VI influences the expression of many nuclear genes, including genes regulated by phytohormones (35, 36) or by reactive oxygen species (44–46). A function of *Arabidopsis* Topo VI as a chromatin-remodeling complex has also been speculated (35). This hypothesis has since been supported by the observation that loss of the Topo VI B subunit in *hlq* mutant plants leads to the misexpression of numerous adjacent genes, hence possibly triggering positional or chromatin context-dependent transcriptional defects (36). This is further supported by the implication of the BIN4 subunit in heterochromatin organization, as observed by smaller and diffuse chromocenters in interphase nuclei of plants bearing the severe *mid* mutation (39).

Here, we reveal that *Arabidopsis* Topo VI is required for chromocenter formation and for efficient silencing of some heterochromatic TEs but has an antagonistic effect on genes localized in EIs. Down-regulation of EI genes in Topo VI mutant plants is associated with an enrichment of the H3K9me2 heterochromatic mark. We further report that the BIN4 subunit of Topo VI directly interacts with S-adenosylmethionine (SAM) synthetase 3/methionine adenosyl transferase 3 (MAT3). Similar to Topo VI knockdown (KD) plants, *mat3* KD mutants exhibit de-repression of heterochromatic TEs and a decrease in H3K9me2. Furthermore, we show that the association of MAT with heterochromatic elements is reduced in a hypomorphic Topo VI mutant, whereas it increased at some EIs. We therefore propose that Topo VI has a prominent role in the delimitation of chromatin boundaries, could participate in defining SAM synthesis sites onto specific regions of the genome, and collectively has an essential role in the establishment of distinct chromatin domains.

Results

Topo VI Is Required for Heterochromatin Organization. Kirik et al. (39) reported that interphase nuclei of the severe *mid* mutant in the BIN4/MID subunit present smaller and less defined chromocenters compared to the WT, suggesting that heterochromatin organization is affected by the *mid* mutation. However, this phenotype was not reported in the allelic *bin4-1* mutant, which also has a severe phenotype (38). Therefore, to unequivocally confirm the role of the *Arabidopsis* Topo VI complex in nuclear organization, we analyzed the nuclear phenotypes of hypomorphic and amorphic mutants of the AtTOP6A subunit, *caa39* and *rhl2-1*, and of the BIN4/MID subunit, a *BIN4* KD line (see below) and *bin4-1*, by DAPI DNA staining and immunolocalization of heterochromatin hallmarks. Both the *caa39* and *rhl2-1* mutants exhibited strong alterations in heterochromatin organization with largely decondensed chromocenters (Fig. 1 *A*, *Top*, and *SI Appendix*, Fig. S1*A*). Likewise, nuclei of epidermal and mesophyll cotyledon cells from *BIN4* KD and *bin4-1* did not harbor conspicuous chromocenters (*SI Appendix*, Fig. S1*A*), as previously reported for the *mid* allelic mutants (39). In contrast, the nuclear phenotype of shoot apical meristematic cells was similar in WT, *caa39*, *rhl2-1*, *bin4-1*, and *BIN4* KD lines, with equal proportions of nuclei with conspicuous (type 1) or diffuse (type 2) chromocenter profiles (*SI Appendix*, Fig. S1*A*, *Bottom*, and *B*). Consistent with its role in endocycles but not in mitosis (31, 37–39), these defects indicate that Topo VI is required for chromatin organization of differentiated cells, but less of actively dividing cells. Immunofluorescence analysis of the heterochromatin hallmark H3K9me2 confirmed the large extent of heterochromatin decondensation in *caa39* Topo VI mutant plants (Fig. 1*A*). Immunoblot analyses further showed that the global level of H3K9me2 is not affected in *caa39* seedlings (Fig. 1*B*). Likewise, 5-methylcytosine (5-meC) immunolabeling also revealed a dispersed signal in *caa39* nuclei (Fig. 1*C*), whereas an anti–5-meC ELISA showed overall similar levels of 5-meC in WT and *caa39* as compared to *ddm1-8* seedlings (Fig. 1*D*). These results suggest that the marked alteration of chromocenter morphology does not result from a global decrease in heterochromatin hallmarks in *caa39*.

Topo VI Is Required for the Silencing of Heterochromatic TEs. A role for *Arabidopsis* Topo VI in heterochromatin-dependent transcriptional gene silencing was highlighted by the reactivation of *TRANSCRIPTIONALLY SILENT INFORMATION* (*TSI*) in *mid* mutant plants (39). However, reactivation was not observed in the *bin4-1* allelic mutant (38). Therefore, to unambiguously assess the involvement of Topo VI in transcriptional silencing and get a more global understanding of Topo VI influence on TE repression, we performed a RNA-sequencing (RNA-seq) analysis of *caa39* and WT transcripts. Multiple heterochromatic TEs (176 TEs with $\log_2$ fold-change [FC] > 2), particularly from the long terminal repeat (LTR)/Gypsy, LTR/Copia and En-Spm/CACTA superfamilies (47), are reactivated in *caa39* plants (Fig. 2*A* and Dataset S1). Conversely, 91 TEs are repressed in *caa39* [$\log_2$(FC) < −2]; unlike reactivated TEs, these repressed TEs are rarely in the most inaccessible and repressive heterochromatin state 9 (*SI Appendix*, Fig. S2*A*). To test for TE silencing defects in other Topo VI mutants, we selected several de-repressed heterochromatic TEs loci (Dataset S1) for which robust primer design was feasible, and measured their relative transcript abundance by qRT-PCR in *rhl2-1* and *bin4-1* mutants along with the *caa39* and WT

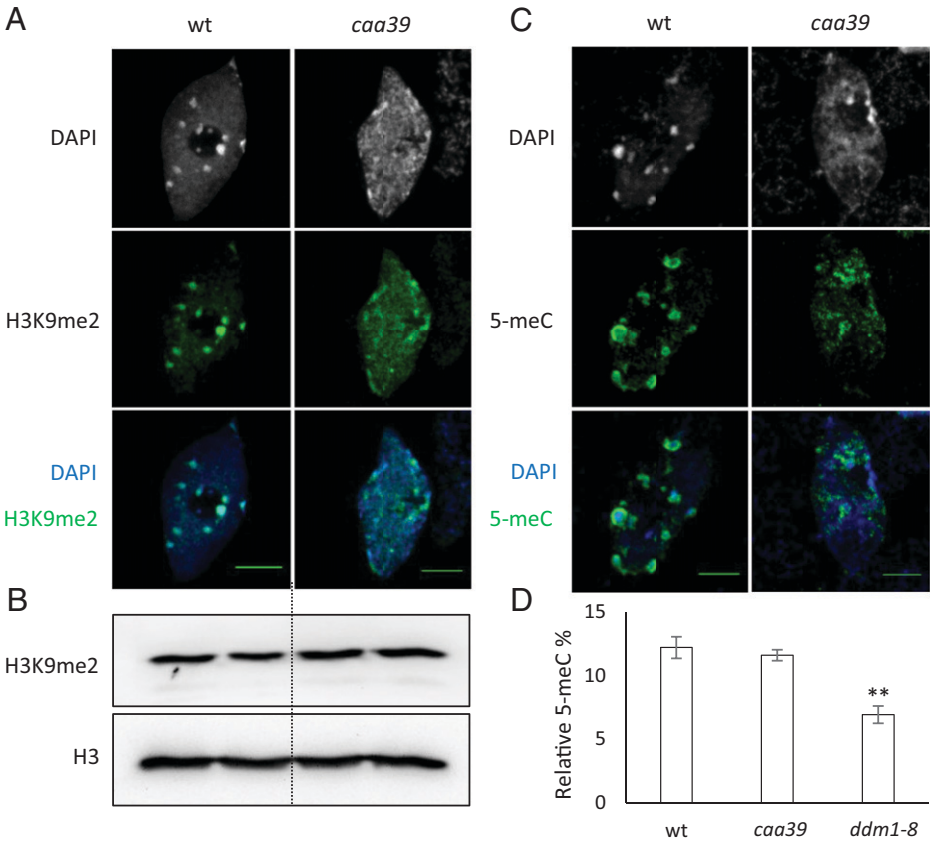

Fig. 1. Topo VI is required for heterochromatin organization. (*A*) Representative nucleus ($n > 30$) from 6-d-old WT and *caa39* cotyledon epidermal cells stained with DAPI and showing indirect immunolocalization of H3K9me2. (Scale bars, 5 μm.) (*B*) Two independently prepared nuclear extracts of WT and *caa39* were immunoblotted against H3 or H3K9me2, as indicated. (*C*) Same as *A* for 5-meC localization. (*D*) Elisa assay to quantify total 5-meC in 6-d-old cotyledons of WT, *caa39*, and *ddm1-8*. $^{**}P < 0.005$ (Student's *t* test).

lines. A clear increase in TE transcript abundance was observed for all three tested Topo VI mutant lines (Fig. 2*B*).

Although we found no global decrease of H3K9me2 and 5-meC in *caa39* (Fig. 1 *B* and *D*), more subtle local changes could account for TE reactivation. We first assessed DNA methylation levels at individual TEs in Topo VI mutants as compared to WT and *ddm1-8* plants by digestion with the methylation-dependent restriction enzyme McrBC. As expected, very efficient digestion of TEs was observed in WT but not in *ddm1-8* plants, reflecting a nearly complete loss of DNA methylation over multiple TEs in this hypomethylated mutant line (Fig. 2*C*). In sharp contrast, we observed WT levels of DNA methylation for all tested loci in *caa39* and *bin4-1* plants. This trend was confirmed in different sequence contexts (CG, CHG, and CHH) by using the methylation-sensitive restriction enzymes HpaII, MspI, and HaeIII (*SI Appendix*, Fig. S3). Similar DNA methylation levels of TEs in WT and *caa39* were then confirmed genome-wide by whole-genome bisulfite sequencing, in all three contexts (Fig. 2*D*). We concluded that TE de-repression in Topo VI mutants could not be accounted for by a global decrease of DNA methylation in *cis*. Next, we measured the level of H3K9me2 at TEs, which could be performed only with the *caa39* hypomorphic mutant, because of the extreme dwarf phenotype of the *rhl2-1* and *bin4-1* null mutants. Chromatin immunoprecipitation (ChIP)-qPCR analyses revealed a modest decrease in H3K9me2 at some but not all tested TEs in *caa39* as compared to WT plants (Fig. 2*E*). ChIP-sequencing (ChIP-seq) analysis of H3K9me2 levels in WT and *caa39*, normalized to H3 levels in each line, confirmed the slight decrease of H3K9me2 at *AT3TE60425* and *AT4TE15030*, but not at *AT2TE15415* and *AT4TE16900* (*SI Appendix*, Fig. S2 *B* and *C*), and revealed a significant global decrease ($P < 0.01$, Mann–Whitney *U* test) of H3K9me2 at TEs (Fig. 2*F*). Collectively, these results suggest that H3K9me2 local decreases and heterochromatin spatial reorganization may contribute to TE activation, although the precise causal mechanism is unknown.

Unlike TEs, Genes Interspersed within Pericentromeric and Chromosome 4 Knob Large Heterochromatin Regions Are Massively Down-Regulated in Topo VI Mutants. We then used the online positional gene-enrichment tool (48) to investigate the genomic distribution of misregulated genes identified in our RNA-seq analysis of *caa39* (Dataset S2). This analysis revealed that the 500 most down-regulated genes are strikingly overrepresented in pericentromeric regions and in the heterochromatic knob of chromosome 4 (*hk4S*) (Fig. 3*A*). In these regions, 94% (181 of 193) of the non-TE genes that are differentially expressed in *caa39* are down-regulated (Dataset S2). In contrast, the 500 most highly up-regulated genes displayed no preferential localization (*SI Appendix*, Fig. S4*A*). To determine whether this effect is robust in other Topo VI mutant lines, we first examined the expression profiles of *bin4-1* and a second allelic mutant, *bin4-2*, from microarray data that were generated during the initial characterization of these two allelic lines (38). Despite the fact that *bin4-1* and *bin4-2* are knockout mutants that have much more severe developmental defects than *caa39*, and although two different technical platforms have been used (RNA-seq for *caa39* vs. Affymetrix ATH1 microarrays for *bin4-1* and *bin4-2*), we found a good correlation between the different transcriptomes (*SI Appendix*, Fig. S4*B*). In particular, 91%

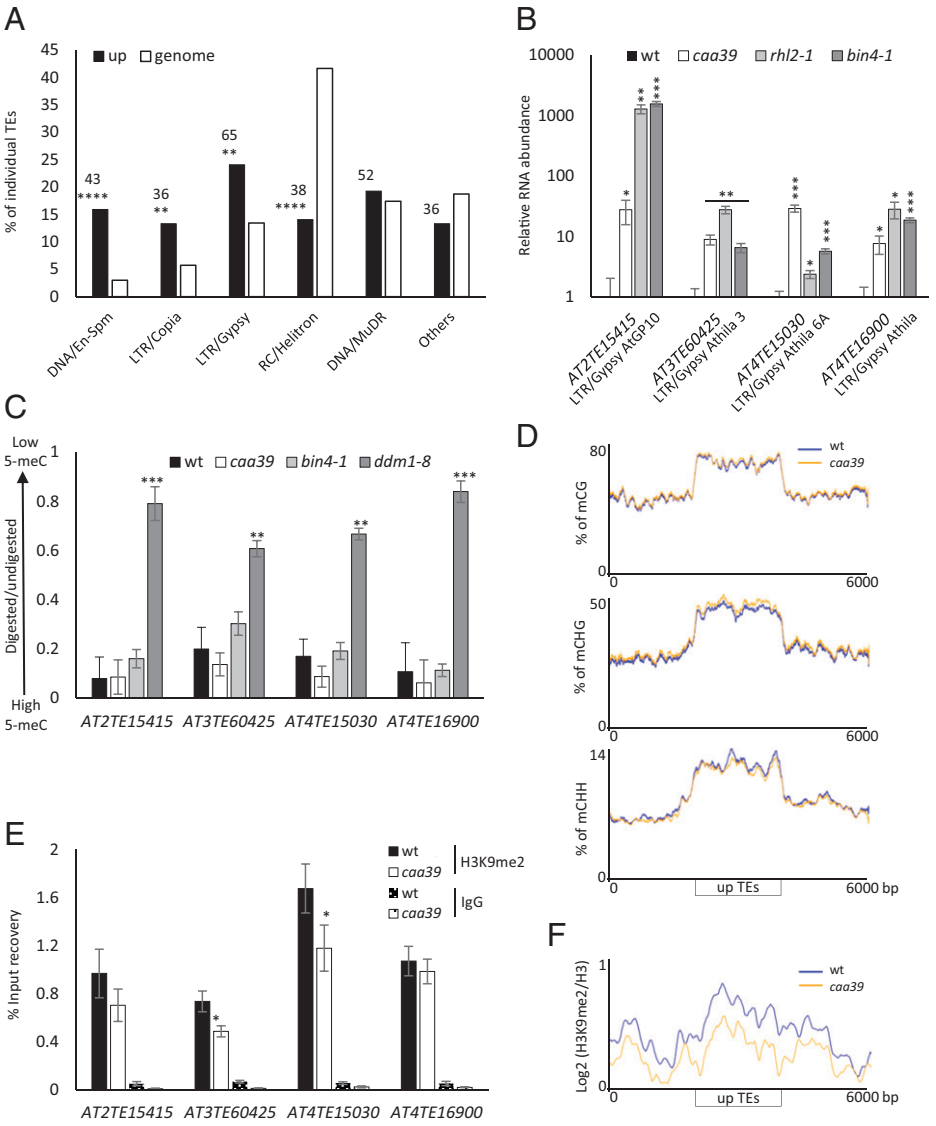

Fig. 2. Topo VI is required for the silencing of transposable elements. (*A*) Bar chart showing the proportions of reactivated TE superfamilies in *caa39* compared to the general proportion of TEs in the genome. The relative percentage is shown for each superfamily and the absolute number of reactivated TEs is noted above each bar. $^{**}P < 0.005$, $^{****}P < 0.0001$ (χ^2 test). (*B*) qRT-PCR confirmation of the reactivation of selected TEs in *caa39*, *rhl2-1*, and *bin4-1*. Error bars: ±SEM of three biological replicates. $^{*}P < 0.05$, $^{**}P < 0.005$, $^{***}P < 0.0005$ (Student's *t* test). (*C*) DNA from indicated genotypes were extracted and digested with McrBC. The mean ratio of digested over undigested DNA from three biological replicates is shown. Error bars: ±SEM of three biological replicates. $^{**}P < 0.005$, $^{***}P < 0.0005$ (Student's *t* test). (*D*) Average distribution of methylated cytosine in CG, CHG, and CHH contexts over TEs and 2-kb flanking regions. Two independent replicates for each genotype were performed. (*E*) ChIP-qPCR of H3K9me2 at selected TEs. Error bars: ±SEM of three biological replicates. $^{*}P < 0.05$ (Student's *t* test). (*F*) Average distribution of H3-normalized H3K9me2 over TEs and 2-kb flanking regions. Two (H3) and three (H3K9me2) independent biological replicates for each genotype were performed.

(72 of 79) of the pericentromeric region genes that are repressed in *caa39* and are detected in both RNA-seq and microarray experiments are also down-regulated in *bin4-1* or *bin4-2* (Fig. 3*B* and Dataset S2). We examined further the expression of seven pericentromeric genes distributed over the five chromosomes and strongly repressed in *caa39*, by qRT-PCR in *caa39*, *bin4-1* as well as in *rhl2-1* plants. These genes were found to be down-regulated in all mutants, except for *AT4G06634* and *AT4G07390* that were not significantly repressed in *rhl2-1* and *bin4-1* (Fig. 3*C*). This could possibly be due to secondary effects of the *bin4-1* and *rhl2-1* amorphic mutations as compared to the less severe *caa39* mutation. In order to test this hypothesis, we took advantage of the availability of an *Arabidopsis BIN4* cosuppressed transgenic line identified during the process of generating lines overexpressing *BIN4-CFP*. Rather than exhibiting *BIN4* up-regulation, this *BIN4* KD homozygous, monoinsertional transgenic line, shows down-regulation of *BIN4* (*SI Appendix*, Fig. S5 *A* and *B*) and develops a phenotype similar to *caa39* (*SI Appendix*, Fig. S5*C*). In this line, all tested pericentromeric genes were at least as much down-regulated as in *caa39*, with a more pronounced effect than in the *bin4-1* and *rhl2-1* knockout mutants (Fig. 3*C*). These observations indicate that Topo VI is required to maintain transcriptional control of both genes and TEs in pericentromeric and *hk4S* regions, possibly acting as a chromatin architectural factor.

Down-Regulated Genes within Heterochromatic Regions Are Localized in Small EIs. We then asked whether the inverse expression patterns of genes and TEs in pericentromeric and *hk4S* regions in Topo VI mutants could be ascribed to their different chromatin landscapes. We first inspected the individual chromatin landscape of the seven down-regulated pericentromeric genes confirmed by qRT-PCR (Fig. 3*C*), using the nine

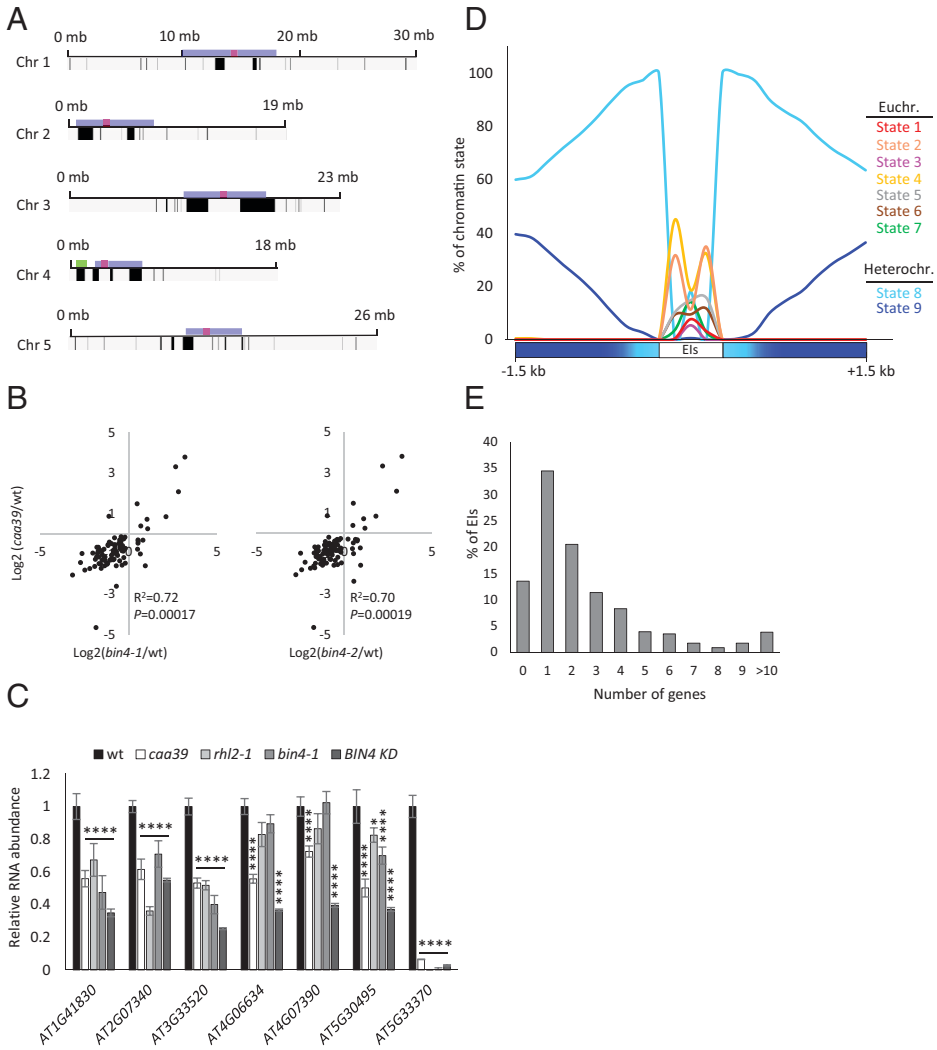

Fig. 3. Genes in EIs within heterochromatic pericentromeric and chromosome 4 knob regions are repressed in Topo VI mutants. (*A*) Positional gene enrichment analysis of the top 500 most down-regulated genes in *caa39*. The bed files corresponding to coordinates of the widest enriched regions (false-discovery rate < 0.05) were visualized with a genome browser. Black lines correspond to enriched regions, blue boxes correspond to pericentromeric regions as defined by Yelina et al. (76), green box to the knob and red to centromeres. (*B*) Scatter plots and Pearson correlations of differentially expressed ($P < 0.05$) pericentromeric genes in *caa39* and *bin4-1* or *bin4-2*. (*C*) qRT-PCR of selected pericentromeric genes in *caa39*, *rhl2-1*, *bin4-1*, and *BIN4* KD at 6 d postgermination. Error bars: ±SEM of three biological replicates. *$P < 0.05$; ****$P < 0.0001$ (two-way ANOVA, Dunnett's test). (*D*) The proportion of each chromatin state was computed for EIs and their 1.5-kb flanking regions. (*E*) Gene content in EIs.

chromatin states defined by Sequeira-Mendes et al. (49). Euchromatin states 2, 1, and 3 characterize the proximal promoter, the transcriptional start site, and the start of coding sequence, respectively. The intragenic states 6 and 7 are characteristic of the transcriptional termination site and gene body of long transcribed genes, respectively. States 4 and 5 are highly enriched in H3K27me3 (a *Polycomb*-Repressive Complex 2 [PRC2]-based repressive histone modification) and are usually found in intergenic regions and PRC2-targeted genes. Finally, the two types of heterochromatin states, 8 and 9, are enriched in H3K9me2, but in contrast with state 8, state 9 preferentially defines pericentromeric heterochromatin and is devoid of H3K27me3 (49). Strikingly, all inspected loci share common features: a typical euchromatin context whose proximal environment is composed of heterochromatic state 8 and whose distal environment is of heterochromatic state 9 (*SI Appendix*, Fig. S6*A*). Overall, these observations suggested that *caa39* down-regulated genes might be part of bona fide EIs.

To generate a comprehensive view of their structural features in the genome, we systematically investigated the pericentromeric and *hk4S* heterochromatic regions defined in *SI Appendix*, Fig. S6*B*. We designed a script to extract all EIs surrounded by chromatin states 8 and 9, then we analyzed the proportion of chromatin states covering EIs and their 1.5-kb flanking regions (Fig. 3*D*). We identified 232 EIs containing 540 EI genes this way, among which 6 correspond to unsequenced gaps (https://jbrowse.arabidopsis.org/?data=Araport11) and were discarded in subsequent analyses (Dataset S3). Looking for EIs directly flanked by state 9 chromatin did not increase the number of EIs identified, showing that chromatin state 8 is always present in the proximal border (Fig. 3*D* and *SI Appendix*, Fig. S6*C*). In contrast, the number of detected EIs started to decrease to 215 when considering 2-nucleosome-long flanking regions in state 8, suggesting that 11 EIs have only one proximal nucleosome in state 8 (*SI Appendix*, Fig. S6*C*). With respect to state 9, the number of extracted islands began to drop from 4-nucleosome-long flanking regions, suggesting that the state 8 proximal border is always flanked by at least 3-nucleosome-long state 9 regions (*SI Appendix*, Fig. S6*C*). A majority of EIs (157 of 232) are short and contain only one or two genes (Fig. 3*E*, *SI Appendix*, Table S1, and Dataset S3).

Topo VI Prevents the Spreading of H3K9me2 into EIs. Given the general repression of EI genes and the local decrease of H3K9me2 at some TE loci without affecting the global level of H3K9me2 (Fig. 1*B*), we hypothesized that EI gene repression might result from ectopic spreading of this silencing mark over EIs. This was first tested on several EI genes by ChIP-qPCR analysis of H3K9me2 levels in WT and *caa39*. H3K9me2 levels were very low, barely above background, in WT, consistent with the fairly high level of expression of these genes (Fig. 4*A*). In contrast, a clear increase of H3K9me2 was observed in *caa39* (Fig. 4*A*). Therefore, we further tested the spreading of H3K9me2 over EIs on a genome-wide scale by ChIP-seq analysis of H3K9me2 levels in WT and *caa39*, normalized to H3 levels in each line. Analysis of the WT profile showed short EIs (S-EIs, which contain only one or two genes and are <6-kb long) with sharp boundaries and where H3K9me2 was barely detected, flanked by regions with high H3K9me2 levels (Fig. 4*B*). Consistent with the minor decrease observed only on some TEs presented in Fig. 2, the H3K9me2 level is globally not lower in EI-flanking sequences in *caa39* as compared to WT. In contrast, a clear increase was observed within S-EIs of *caa39*, which was highly significant all along S-EIs (Mann–Whitney *U* test, Benjamini-corrected $P < 0.01$), suggesting that Topo VI prevents H3K9me2 spreading across natural boundaries (Fig. 4*B*). H3K9me2 spreading into large and more complex EIs (L-EIs, >6-kb long and often containing internal state 8) was also highly significant and particularly pronounced on L-EIs boundaries (Fig. 4*C*). Inspection of metaprofiles for each chromosome confirmed highly significant H3K9me2 spreading into EIs (*SI Appendix*, Fig. S7*A*), that was observed for all replicates (*SI Appendix*, Fig. S7*B*).

To further strengthen our analysis, we applied diffReps (50) on each replicate individually to confirm differential enrichment of H3K9me2 in EIs of *caa39* and WT (Dataset S4). This very stringent and not very sensitive analysis (essentially due to the fact that H3K9me2 peaks were barely detectable in WT and that H3K9me2 spreading does not appear to be sequence-specific) could still reveal increased levels of H3K9me2 in some EIs of *caa39*, but not all (92.0% in replicate 2, 73.9% in replicate 3, 27.4% in replicate 1) (Dataset S3). The limited number of EIs identified this way in replicate 1 can be attributed to the fact that it was less deeply sequenced than replicates 2 and 3 (GSE103924). Despite that, there was a large overlap between replicates: among EIs that showed increased levels of H3K9me2 in *caa39*, only one was identified in replicate 1 but not in replicates 2 or 3, and 96.4% (161 of 167) of the EIs identified in replicate 3 were also identified in replicate 2 (*SI Appendix*, Fig. S7*C* and Dataset S3). We then extracted the number of significantly (diffReps G-test, $P < 0.01$) up or down H3K9me2 peaks in *caa39* versus WT, in each individual replicate (Dataset S4). A similar percentage of significantly up or down H3K9me2 peaks was observed at the genome scale by this method (Fig. 4*D*), in agreement with the fact that the global level of H3K9me2 does not seem to be significantly affected in *caa39*. In contrast, the proportion of peaks was significantly shifted toward gains of H3K9me2 within EIs, particularly within EI genes and their 5′ UTRs (Fig. 4*D* and Dataset S4), confirming the specific role of Topo VI in safeguarding EI genes from ectopic spreading of H3K9me2.

Globally, these data show that Topo VI is required to prevent elevated H3K9me2 levels within EIs, presumably by preserving sharp boundaries between these insulated elements to avoid pervasive spreading of heterochromatin from flanking regions. We further documented such a barrier-like function on an S-EI containing a single gene, *At1g41830*, by ChIP-qPCR analysis of H3K9me2. Scanning of six different loci along this region (Fig. 4*E*) in independent experiments confirmed the increased H3K9me2 levels within the island body, but also a decrease in one neighboring heterochromatic border (Fig. 4*E*), similarly to what was observed in the ChIP-seq experiment replicates for this EIs (Fig. 4*I* and *SI Appendix*, Fig. S8) and other inspected EIs (*SI Appendix*, Fig. S8).

EI Gene Repression Is Correlated with H3K9me2 Spreading. We then tried to evaluate the relative contribution of H3K9me2 increase to the down-regulation of EI genes, compared to other heterochromatin and repressive marks. First, because H3K9me2 and non-CG (CHG and CHH) DNA methylation are strongly interdependent (51), we tested whether H3K9me2 spreading into EIs might in turn, or reciprocally, affect DNA methylation. Whole-genome bisulfite sequencing revealed that DNA methylation levels in all sequence contexts were overall unaltered in *caa39* relative to WT in EIs (Fig. 4 *F* and *I* and *SI Appendix*, Fig. S8). Differentially methylated region (DMR) analyses confirmed that there was no global significant increase of DNA methylation in EIs (Dataset S5). Surprisingly, despite CHGs being known to be methylated through a feedback loop with H3K9me2, DMR analyses rather revealed a very slight decrease of CHG, with 51 hypo-CHG DMRs and 16 hyper-CHG DMRs observed in EIs of *caa39* (with differences in the methylation percentage higher than 10%, $P < 0.05$) (Dataset S5). Therefore, DNA methylation does not seem to contribute to the down-regulation of gene expression in EIs.

Second, because EI boundaries are enriched in H3K27me3-marked heterochromatin state 8, and that H3K27me3 is also found on the proximal promoter (chromatin state 2) and transcribed region of many euchromatic genes (chromatin state 5, silenced genes) (49), we also performed a genome-wide H3K27me3 analysis by ChIP-seq. Interestingly, we observed a globally inverted tendency as compared to H3K9me2 profiles: average H3K27me3 levels were locally and significantly decreased within EIs (*SI Appendix*, Fig. S9 *A* and *B*). We further documented such a local decrease of H3K27me3 on the S-EI containing *At1g41830*, by ChIP-qPCR (*SI Appendix*, Fig. S9*C*). Consistent with this, K-means linear clustering revealed that H3K27me3 decrease could not be generalized to all EIs, as it marks only a small subset of EIs in WT (Fig. 4*G*). Thus, H3K27me3 does not seem to contribute to the global down-regulation of EI genes, and its local decrease at some EI genes might even counterbalance the effect of H3K9me2 increase in a few EIs.

Finally, we directly compared EI gene expression with H3K9me2 changes. A vast majority (90%) of EI genes that show significant changes ($P < 0.05$) in either RNA-seq or ChIP-seq analyses are repressed and possess enhanced levels of H3K9me2 (Fig. 4 *H* and *I* and *SI Appendix*, Figs. S8 and S10*A*). Interestingly, the most repressed genes also tend to have the sharpest H3K9me2 increase, which is particularly true in S-EIs (Fig. 4*H* and *SI Appendix*, Fig. S10*A*). To see whether H3K9me2 defect might affect the expression of EI genes, we generated the quadruple mutant *caa39 suvh456* mutated for the H3K9 methylase genes *KRYPTONITE (KYP)/SUVH4*, *SUVH5*, and *SUVH6* and examined the expression of the seven pericentromeric genes already studied. The expression of some EI genes was significantly increased in *caa39 suvh456* as compared to *caa39* (*SI Appendix*, Fig. S10*B*). Taken together, these results suggest that H3K9me2 increase plays a role in the

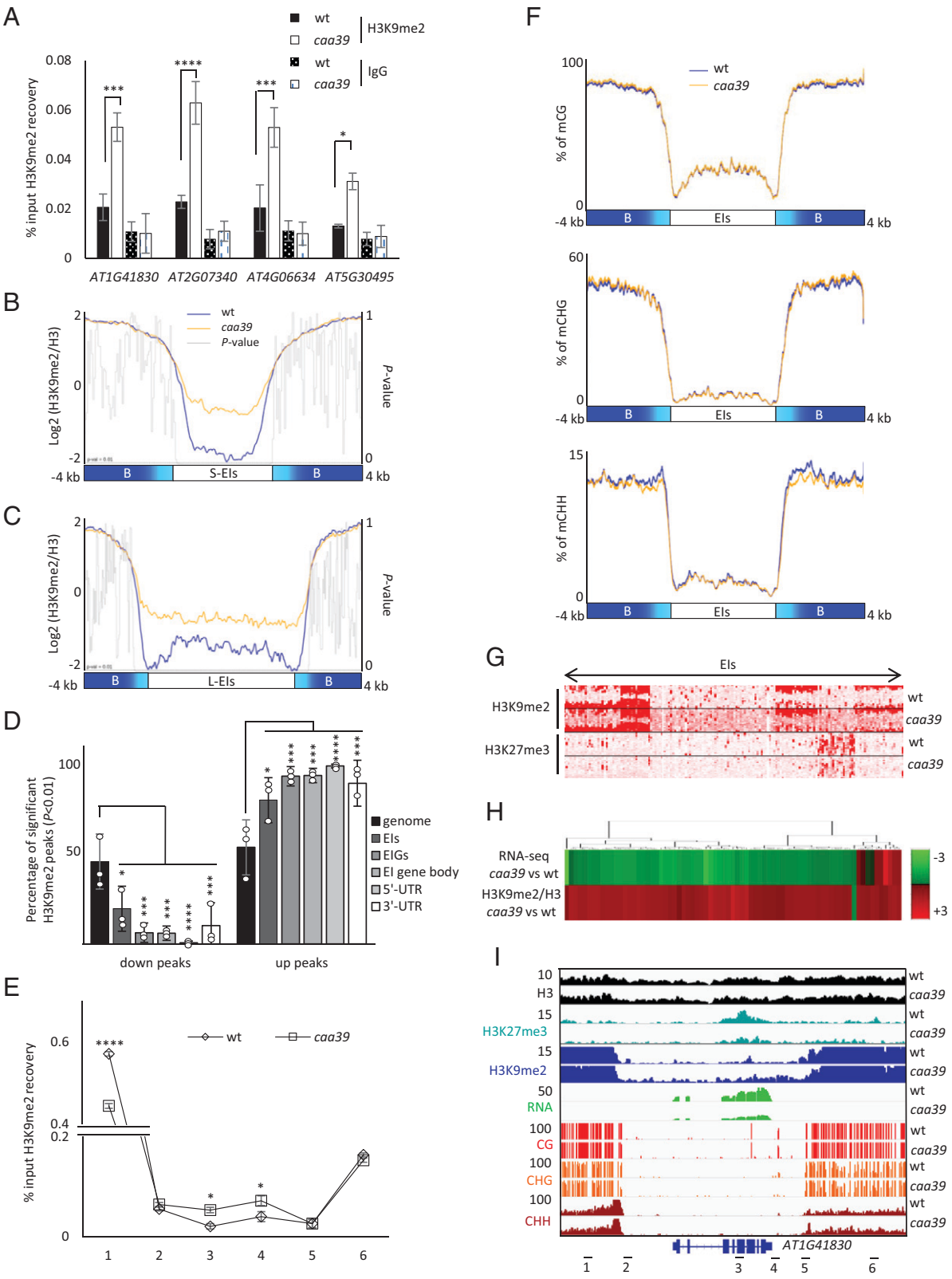

Fig. 4. Topo VI prevents the invasion of EIs by H3K9me2. (*A*) ChIP-qPCR analysis of H3K9me2 at EI genes. Error bars: ±SEM of two biological replicates. *$P < 0.05$, ***$P < 0.0005$, ****$P < 0.0001$ (two-way ANOVA, Fisher's test). (*B*) Average distribution of H3-normalized H3K9me2 along short euchromatic gene islands and 4-kb flanking regions. Two (H3) and three (H3K9me2) independent biological replicates for each genotype were performed. *P* value was computed for each aggregated point by using the Mann–Whitney *U* test. (*C*) Same as *B*, long EIs. (*D*) Bar chart showing the average percentage of down or up H3K9me2 peaks identified by diffReps analysis in the genome, EIs, EI genes (EIGs), EI gene body, 5′ and 3′ UTRs. Error bars: ±SEM of three biological replicates. *$P < 0.05$, ***$P < 0.0005$, ****$P < 0.0001$ (two-way ANOVA, Fisher's test). (*E*) ChIP-qPCR validation of a single-gene island for H3K9me2. Error bars: ±SEM of three biological replicates. *$P < 0.05$, ****$P < 0.0001$ (two-way ANOVA, Fisher's test). (*F*) Average distribution of methylated cytosine in CG, CHG, and CHH contexts over EIs. Two independent replicates for each genotype were performed. (*G*) K-means linear clustering of H3K9me2 and H3K27me3 tag densities across EIs and their 900-nt flanking borders as revealed by seqMINER in *caa39* and WT. (*H*) Heatmap correlation clustering of EI genes with significant changes in RNA-seq and H3K9me2/H3 ChIP-seq. (*I*) Integrative Genomics Viewer (77) screenshot of H3, H3K9me2, H3K27me3, RNA, CG, CHG, and CHH methylation profiles in WT and *caa39* on a single gene-containing island. Each track is normalized against corresponding input samples (ChIP-seq) and by the sequencing depth. Numbers indicate the position of primers used in *E*.

reduced expression of EI genes, although higher-order chromatin structure, changes in other histone modification, and other indirect effects of the *caa39* mutation may contribute to gene expression changes.

The Topo VI Subunit BIN4 Physically Associates with MAT3. To gain knowledge on the molecular mechanism by which Topo VI contributes to the delimitation of chromatin boundaries, we used the BIN4 subunit as a bait to screen a yeast two hybrid (Y2H) cDNA library (Hybrigenics). A strong interaction with the Topo VI subunit RHL1 was detected, thereby demonstrating the reliability of the screening procedure (Dataset S6). Among the 11 additional interacting partners, 3 proteins belong to the SAM biosynthesis pathway, the universal methyl group donor (52). The first one, 5-methylthioribose-1-phosphate isomerase (MTI1, AT2G05830), is involved in the methionine salvage pathway, whereas the two others, methionine synthase 1 (MS1, AT5G17920) and MAT3 (AT2G36880) are the ultimate enzymes of the SAM cycle. In order to identify BIN4-interacting proteins in planta, we also performed a co-IP/mass spectrometry (MS) experiment using the *Arabidopsis mid-1 35S:BIN4/MID-YFP* line, which consists of the *mid-1* allelic mutant of *BIN4* complemented with YFP-tagged BIN4/MID (39), and a WT line as control. To exclude nonspecific proteins, we discarded proteins that were not detected in both BIN4/MID-YFP co-IP/MS replicates, as well as plastidial, mitochondrial, and peroxisomal proteins. The presence of the RHL1 and TOP6B Topo VI subunits in BIN4/MID-YFP co-IPs validated our procedure (Dataset S7). Remarkably, MAT3 coimmunoprecipitated strongly with BIN4. MAT4 also coimmunoprecipitated with BIN4, but apparently to a much lesser extent (Dataset S7). We further investigated the genetic and biochemical interactions between BIN4 and enzymes of the SAM cycle, particularly the very last enzyme MAT3, using bimolecular fluorescence complementation (BiFC). We confirmed the BIN4-MAT3 and BIN4-MS1 interactions in nuclei of transiently agro-transformed *Nicotiana benthamiana* mesophyll cells (Fig. 5*A*).

MAT3 Is Required for H3K9me2. Given that MAT enzymes synthesize the SAM required for DNA and histone methylation, and that Topo VI is required for proper distribution of H3K9me2 throughout EI-containing heterochromatic regions, we hypothesized that disruption of MAT3 affects H3K9me2 deposition. To address this question, we used a recently characterized KD line in which *MAT3* 3′-UTR is interrupted by a T-DNA (53), generating strongly reduced but still detectable transcript levels (*SI Appendix*, Fig. S11*A*). We measured H3K9me2 levels at the four TEs strongly de-repressed in Topo VI mutant plants (Fig. 2) by ChIP-qPCR and found decreased levels of H3K9me2 (Fig. 5*B*). This modest decrease of H3K9me2 might be explained by the hypomorphic nature of the mutation or by a functional redundancy between MAT isoforms that share over 85% amino acid sequence identity (*SI Appendix*, Fig. S11*B*).

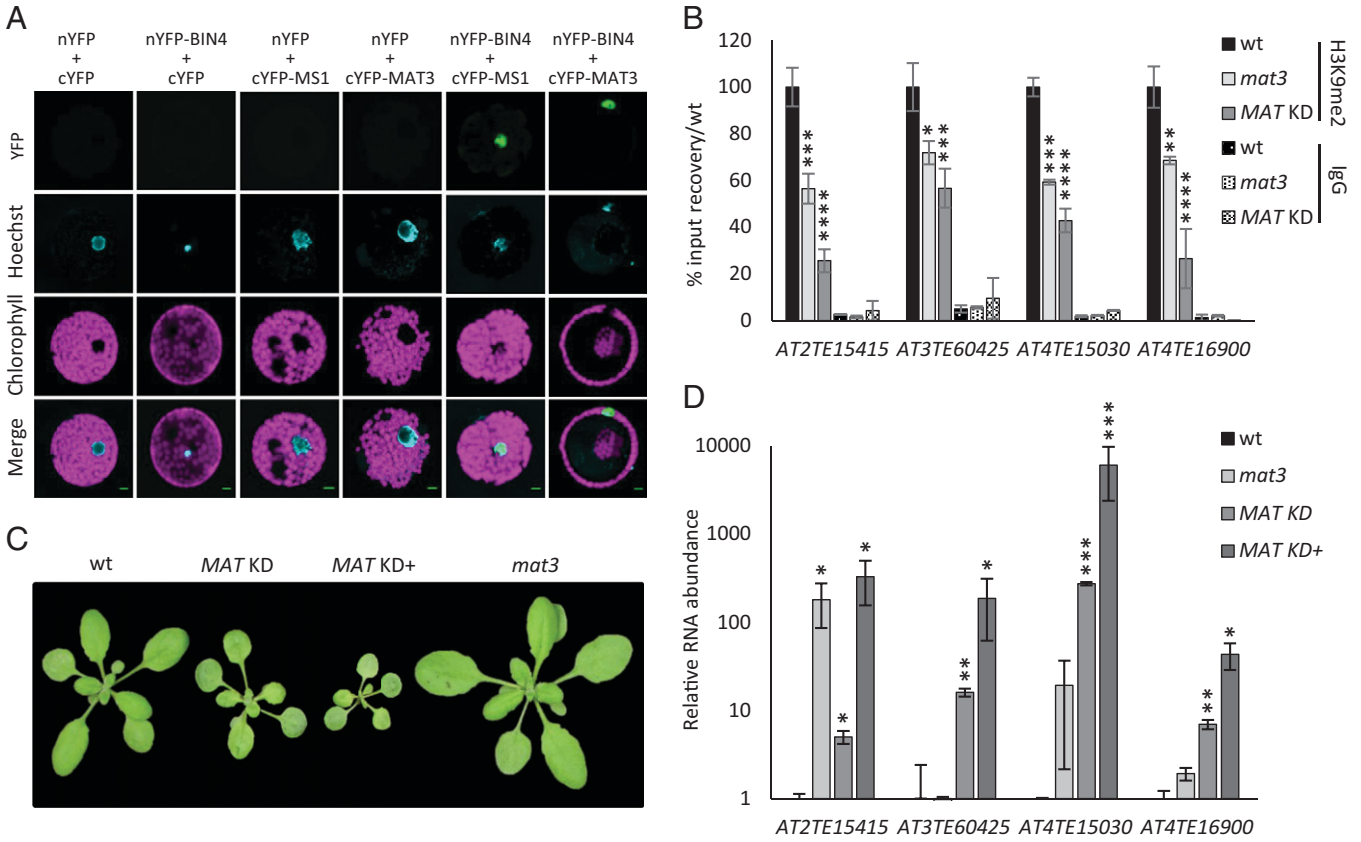

Fig. 5. MAT3 interacts with Topo VI and is required for H3K9me2 deposition on heterochromatic loci. (*A*) Protoplasts from transiently agrotransformed *N. benthamiana* leaves expressing different combination of BiFC vectors, as indicated. Nuclei were stained with Hoechst 33342. (Scale bars, 10 μm.) (*B*) Chromatin of 3-wk-old WT or *MAT* KD (here a mixed pool of *MATs* silenced plants with strong or weak phenotype) rosette leaves, or 6-d-old WT or *mat3* cotyledon nuclei was immunoprecipitated with anti-H3K9me2 antibodies and the recovery of TEs known to be reactivated in *caa39* was assessed by qPCR. The result is shown as a percentage of recovery normalized against WT. Error bars: ±SEM of two biological replicates. **P* < 0.05, ***P* < 0.005, ****P* < 0.0005, *****P* < 0.0001 (two-way ANOVA, Dunnett's test). (*C*) Representative photographs of 4-wk-old WT, *MATs* silenced plants with stronger (*MAT* KD^{+}) and weaker (*MAT* KD) developmental phenotypes, and the *mat3* mutant. (*D*) qRT-PCR analysis of TE transcript abundance in indicated genotypes. Error bars: ±SEM of three biological replicates. **P* < 0.05, ***P* < 0.005, ****P* < 0.0005 (Student's *t* test).

To test this hypothesis, we took advantage of a homozygous, monoinsertional, cosuppressor transgenic line obtained during the process of generating *MAT3-YFP* overexpressors, that we referred to as *MAT* KD (Fig. 5*C* and *SI Appendix*, Fig. S11*C*). Because of their high DNA sequence identity (*SI Appendix*, Fig. S11*D*), all *MAT* genes were down-regulated in this line (*SI Appendix*, Fig. S11*E*). In addition, the stochastic silencing of *MATs* gave rise to different phenotype severities: mildly affected *MAT* KD plants (Fig. 5*C*) that accumulated fewer *MAT*s transcripts than WT (*SI Appendix*, Fig. S11*E*) and presented a more severe phenotype than *mat3* hypomorphic mutant plants (Fig. 5*C*); and strongly affected *MAT* KD^{+} sister plants (Fig. 5*C*) that accumulated even fewer *MAT* transcripts (*SI Appendix*, Fig. S11*E*). As anticipated, the H3K9me2 decrease was even more pronounced in *MAT* KD plants than in *mat3* (Fig. 5*B*). These results suggest that MAT isoforms possibly have additive roles in H3K9 dimethylation. Given the decrease of H3K9me2 in MAT-deficient plants, we then determined the extent of TE reactivation in *mat3* and *MAT* KD by qRT-PCR analysis of the same four TEs. We observed increased levels of TE transcripts in *mat3* (Fig. 5*D*). This increase was generally more pronounced in *MAT* KD plants, particularly in *MAT* KD^{+} plants (Fig. 5*D*). In contrast, we did not observe any significant effect on EI gene expression (*SI Appendix*, Fig. S11*F*).

Topo VI Favors MAT Enrichment at Some Heterochromatin Borders and Depletion from EIs. Collectively, our results suggest that Topo VI and MAT3 could act together in maintaining sharp chromatin boundaries by influencing H3K9me2 deposition. We therefore used a newly developed anti-MAT antibody (Agrisera) to test for MAT enrichment at specific loci and a putative Topo VI dependency. First, the specificity of this antibody was validated by immunoblot analysis of protein extracts from WT, *MAT* KD, and *MAT3-YFP* overexpressing lines (*SI Appendix*, Fig. S12*A*). We then performed ChIP-qPCR using an anti-MAT antibody and chromatin from WT and *caa39* plants, to measure the recovery of TEs that are reactivated upon Topo VI or MATs loss of functions. Interestingly, MATs were enriched on all the tested TEs in WT and less in *caa39*, as compared to an IgG control (Fig. 6*A*). To specifically evaluate the implication of the BIN4/MID-associated MAT3 isoform, we performed ChIP-qPCR using an anti-GFP antibody and chromatin from two independent MAT3-YFP expressing lines. TEs reactivated in *MAT* KD and in Topo VI mutant plants were also specifically enriched in the GFP-pulled down chromatin (*SI Appendix*, Fig. S12*B*). These results indicate that Topo VI is required for the association of MAT3 with heterochromatic elements.

To test whether Topo VI might also influence the enrichment of MATs at EIs, we performed ChIP-qPCR using an anti-MAT antibody and chromatin from WT and *caa39*, and analyzed the same EI as in Fig. 4 *E* and *I*, which shows increased H3K9me2 levels within the island body (probe 3–4) but decreased levels in the 5′ heterochromatic border (probe 1) in *caa39* (Figs. 4 *E* and *I* and 6*B*, *Upper*). We detected a significant decrease of MAT occupancy in this border in *caa39* (Fig. 6 *B*, *Lower*, probe 1) and, conversely, significantly enhanced MAT occupancy in the island body (probe 3) in *caa39* compared to WT (Fig. 6 *B*, *Lower*, probes 3–4). We analyzed three other S-EIs that show decreased gene expression levels (Fig. 3*C*), increased internal H3K9me2 levels (Fig. 4*C* and *SI Appendix*, Fig. S8) and contain a single gene (*At4g06634*'s and *At5g30495*'s EIs) or two genes (*At2g07340*'s EIs). We observed trends of decreased MAT occupancy at one or both borders and enhanced MAT occupancy in the island bodies of *caa39* (Fig. 6 *C*–*E*). These results suggest that the loss of Topo VI leads to MAT redistribution over EIs, which correlates with H3K9me2 redistribution and EIs heterochromatinization in *caa39*.

Discussion

The *Arabidopsis* epigenome is largely indexed by discrete chromatin signatures usually corresponding to single genetic element (e.g., a gene or a TE) (49, 54). However, despite this, in *Arabidopsis* DNA methylation has a known tendency to spread away from many TEs (55), and a few other studies have reported the existence of heterochromatin spreading in plants (56–58). Yet, the mechanisms that repress heterochromatin spreading, hence safeguarding EIs, are poorly understood in plants. Our study confirmed the existence of an insulator-like mechanism that preserves EIs and unveiled the role played by the Topo VI complex in this process. We first provide evidence that Topo VI is required to preserve the euchromatic nature and transcriptional activity of gene islands within pericentromeric and chromosome 4 knob heterochromatic regions. Indeed, the most remarkable effect of the *caa39* mutation was the specific misregulation of pericentromeric elements, with a general down-regulation of EI genes and, inversely, a reactivation of some heterochromatic TEs. We confirmed this peculiar expression pattern in several amorphic and hypomorphic mutants of the Topo VI complex. Surprisingly, EI gene down-regulation is more pronounced in the hypomorphic mutants *caa39* and *BIN4* KD than in the corresponding null Topo VI mutants that display more severe growth defects. Taking advantage of uncoupled growth defects and gene-expression changes in the hypomorphic *caa39* allele, we were able to show that the repression of EI genes is correlated with the invasion of EIs by H3K9me2, indicating that Topo VI is required to prevent the spreading of H3K9me2, here referred to as a boundary function. The increased expression of some EI genes in the quadruple mutant *caa39 suvh456*, defective for the H3K9 methylase SUVH4, SUVH5, and SUVH6, as compared with *caa39*, further supported that H3K9me2 spreading over EI genes participates to some extent in the transcriptional silencing of EI genes in Topo VI-defective plants.

Although it is known that CHG methylation is maintained through a feedback loop with H3K9me2, whole-genome bisulfite sequencing identified no global increase of cytosine methylation over EIs in *caa39,* but rather a slight decrease of CHG methylation, suggesting that DNA methylation is not involved in the reduced expression of EI genes in Topo VI mutants. Other recent work has also shown that, under specific circumstances, increased H3K9me2 levels do not necessarily result in increased CHG or CHH methylation, and vice versa. For example, the AT-hook protein AHL10 ectopically recruits H3K9me2 to small, AT-rich TEs without coincidental increase in DNA methylation (59). Conversely, the expression of *AtCMT3* in *Eutrema salsugineum*, a Brassicaceae that has lost *CMT3* and gene body methylation, induces de novo gene body methylation in CHG, CHH, and CG contexts, but without resulting in stable gain of H3K9me2. Interestingly, CHG hypermethylation in gene bodies is also not correlated with consistent changes in gene expression in this case (60). While DNA methylation does not appear to be involved in the reduced expression of EI genes in Topo VI mutants, the question of the relative importance of H3K9me2 remains. Indeed, and first, the level of H3K9me2 in EIs of *caa39* is still

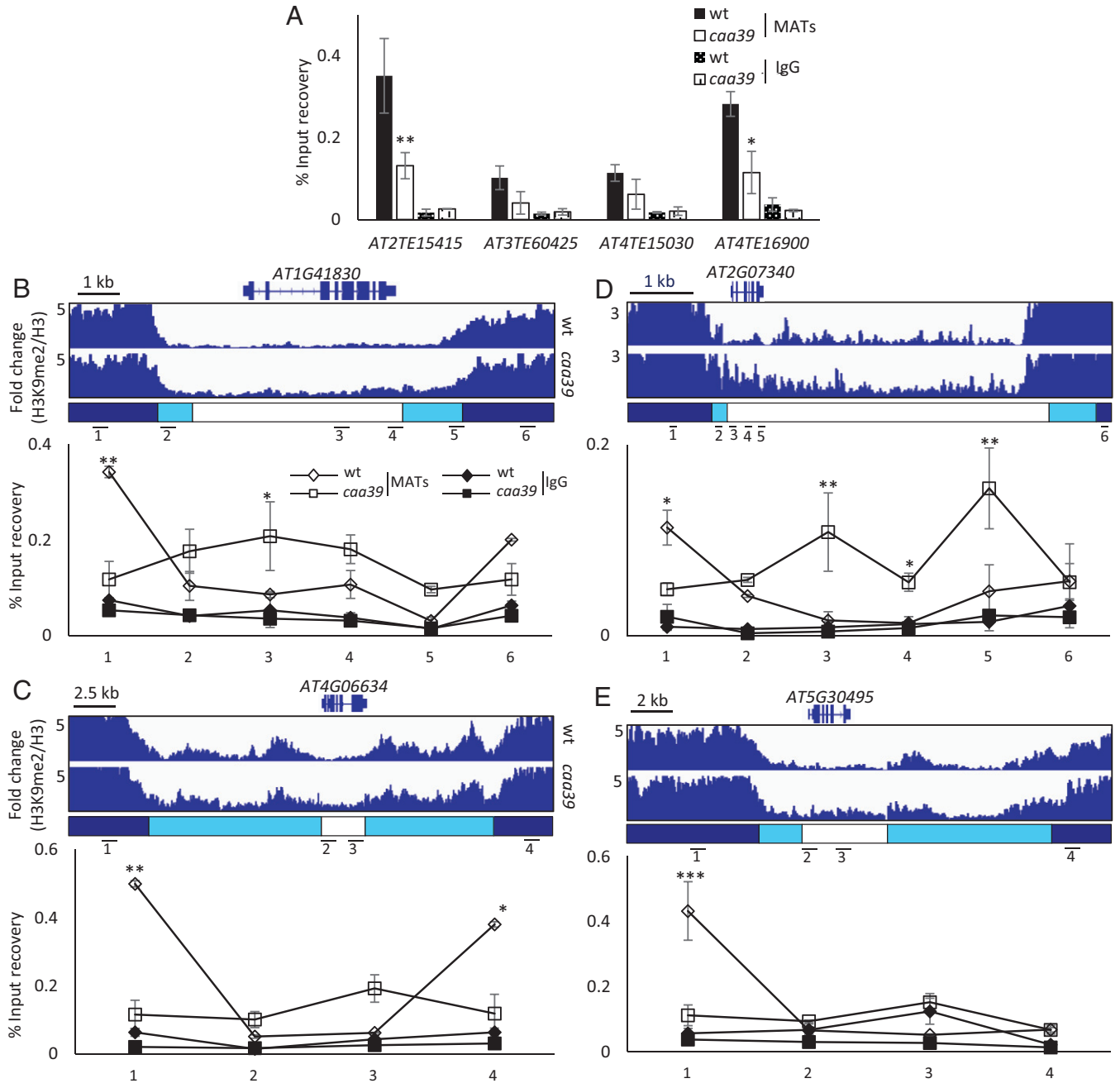

Fig. 6. Topo VI is required for MAT enrichment at heterochromatin borders and exclusion from EIs. (*A*) Chromatin of 6-d-old WT or *caa39* cotyledon nuclei was immunoprecipitated with anti-MATs antibodies and the recovery of TEs reactivated in *MATs* silenced plants and *caa39* was measured by qPCR. Error bars: ±SEM of three biological replicates. (*B–E*, *Upper*) Integrative Genomics Viewer screenshots of H3- and sequencing depth-normalized H3K9me2 profiles, and locations of primers used in *Lower* panels. (*Lower*) Same as *A* on EIs containing repressed genes in *caa39* such as *AT1G41830* (*B*), *AT4G06634* (*C*), *AT2G07340* (*D*), and *AT5G30495* (*E*). Error bars: ±SEM of two biological replicates. **P* < 0.05, ***P* < 0.005, ****P* < 0.0005 (Student's *t* test).

significantly lower than in canonical heterochromatin. This might result from histone H3 demethylation, a process that is likely still active in *caa39*. Alternatively, gain of H3K9me2 could be the outcome of a subset of cells in which *caa39* mutation has a strong effect on H3K9me2 boundaries. Second, the negative correlation between EI gene expressions and H3K9me2 changes is good, particularly in small EIs, but not very high, suggesting that H3K9me2 spreading over EI genes cannot entirely explain the transcriptional silencing of EI genes. H3K9me2 spreading on EIs might, in turn, affect the establishment of other chromatin modifications. For example, in the *ibm1* mutant, increased levels of H3K9me2 on gene bodies are associated with decreased levels of H3K4me1 and transcriptional silencing (61). Conversely, in the *suvh456* triple mutant, many TEs show a drastic increase in H3K4me1 level, which is associated with transcriptional de-repression and loss of H3K9me2 (61). Therefore, it is plausible that other histone methylation changes also occur in *caa39*, as we did observe for H3K27me3, which shows an opposite trend to H3K9me2 in EIs. Thus, H3K9me2 spreading might itself perturb H3K27me3 deposition by PRC2 and erasing by trithorax group (trxG) proteins. This second hypothesis is supported by similar observations made in other organisms, where the loss of Swi6/HP1 leads to H3K9me2 spreading across natural constitutive heterochromatin boundaries in fission yeast (62), and alters H3K27me3 deposition on facultative heterochromatin in *Neurospora crassa* (63).

In animals, insulator proteins like CTCF can participate in several distinct processes, for example, locally as a chromatin barrier and more globally on the formation of topologically associating domains (64). Similarly, the disorganization of chromocenters and the partial loss of pericentromeric TE silencing observed in Topo VI mutants might result from the loss of a local boundary function and, possibly, also by the loss of a distinct, more global, architectural function of Topo VI in heterochromatin condensation. Indeed, given that no obvious loss of DNA methylation and only a partial decrease of H3K9me2 over TEs were observed in Topo VI mutant plants, the reactivation of TEs is unlikely to be solely explained by decreased levels of these marks, but rather by a combined loosening of their heterochromatic nature and of their higher-order organization. Although causal link between chromatin reorganization and TE reactivation in plants is very disputed, a few recent studies link chromatin organizers with TE de-repression independently of DNA demethylation. For example, the natural depletion of histone 1 in sex cells is responsible of the reactivation of approximately 100 heterochromatic TEs via DNA demethylation-dependent (77 of 98) and -independent (21 of 98) mechanisms (65). In addition, MORC proteins, which belong to the GHKL ATPases superfamily like Topo VI, are required for the silencing of approximately 20 TEs and the formation of chromocenters without impacting H3K9me2 and DNA methylation levels (66–68). Interestingly human CTCF has been shown to interact with Topo IIβ (69, 70) and appears to be part of a protein interaction network that also contains MORC2 and members of the cohesin complex in HeLa cells (71). Intriguingly, plant and human recombinant MORC proteins seem to display a type II topoisomerase-like activity, which requires additional plant extracts for full activity (72).

Given the function of MAT enzymes in the synthesis of SAM, MAT perturbation is expected to affect a wide range of methylation reactions, which include DNA and histone methylations. The *mat3* mutant line used in our study has been shown, however, to have global SAM levels similar to WT and only very slightly reduced global levels of DNA methylations, unlike other *mat* mutants that show more severe DNA and histone methylation defects (73). This suggests that the increased levels of some TE transcripts in *mat3*, and the corresponding decreased levels of H3K9me2, are more likely attributable to a local effect of the *mat3* mutation, rather than a global decrease of SAM, or be the outcome of a subset of cells in which *mat3* mutation has a strong effect. Our finding that the Topo VI BIN4 subunit directly interacts with MAT3 and is required for MAT3 enrichment at some TE loci and depletion from euchromatic islands, might provide a mechanistic explanation for such a local role of MAT3 on chromatin, in addition to its general role in SAM synthesis (73). Similarly, the mammal MATIIα isoform also directly supplies SAM in the close vicinity of oncogenes to allow transcriptional repression and H3K9me2 deposition (74, 75). Intriguingly, the mouse MATIIα has been found to interact with Topo IIα, a type IIA topoisomerase whose C-terminal regulatory domain possesses sequence similarity with the BIN4 subunit of the plant Topo VI complex (38). Hence, although this requires testing in other organisms, an interaction between MAT enzymes and type II topoisomerases might be evolutionary conserved. Targeting of MATs to specific chromatin regions by topoisomerases might be a way to couple SAM synthesis and availability in situ, possibly for DNA or histone methylation. Extensive genome-wide studies will provide a general view of chromatin modification changes in different *mat* mutants and their relative impacts on TE and gene expression.

In plants, the existence of an insulator-like function that would partition chromatin into different functional domains has long been questioned (9, 11, 26). We show that Topo VI participates to such a function by preventing the spreading of the heterochromatic mark H3K9me2 into neighboring euchromatin islands. Our results suggest that the prevention of heterochromatin spreading might rely upon a Topo VI–MAT3 interaction that would be important for the proper targeting of MAT3 to heterochromatin and its exclusion from EIs. Future studies might allow the identification of direct molecular links between Topo VI, MAT proteins, and methyltransferases involved in DNA and histone methylation, for fine-tuning the establishment of sharp transitions in chromatin identity along the genome.

Materials and Methods

Detailed descriptions of the experimental methods are provided in *SI Appendix, SI Materials and Methods*. These include cloning procedures, plant material and growth conditions, DNA preparation, Chop- and ChIP-qPCR, anti–5-meC ELISA, Y2H screen, co-IP/MS, Western blot, RNA extraction, qRT-PCR and microarrays, RNA-seq library preparation and sequencing, RNA-seq bioinformatic treatment and analysis, whole-genome bisulfite sequencing, and DNA methylation analysis, ChIP, ChIP-seq analysis, immunofluorescence, transient transformation and protoplasts preparation, confocal and epifluorescence microscopy.

Data Availability. ChIP-seq, RNA-seq, bisulfite sequencing, and microarray datasets have been deposited in the Gene Expression Omnibus (GEO) database, https://www.ncbi.nlm.nih.gov/geo (accession no. GSE129249). Custom scripts used in this study are available in GitHub at https://github.com/michel-teresse.

ACKNOWLEDGMENTS. We are indebted to Michel Térèse for his valuable help in writing scripts for bioinformatic analyses. We thank Imen Mestiri (Institut de Biologie de l'École Normale Supérieure, Paris) for her expertise with cytogenetics; students who contributed to this work, especially Justine Quillet, Julien Vieu, and César Botella; and Ben Field for critical reading of the manuscript. This work was supported by French National Research Agency ANR 2010-JCJC-1205-01 and ANR-14-CE02-0010 (to C. Laloi). Work by F.B. was supported by French National Research Agency ANR-10-LABX-54, ANR-18-CE13-0004-01, ANR-17-CE12-0026-02, and by Velux Stiftung (Switzerland). L.D. was supported by the Commissariat à l'énergie atomique et aux énergies alternatives and Région Provence-Alpes-Côte d'Azur. F.V. is a recipient of a PhD fellowship from the French Ministry of Higher Education, Research and Innovation. High-throughput RNA-sequencing was performed at the POPS platform, supported by the LabEx Saclay Plant Sciences-SPS (ANR-10-LABX-0040-SPS). Mass spectrometry analysis was performed at the IMM platform supported by a grant from the Groupement d'Intérêt Scientifique (GIS) Infrastrutures en Biologie Sante et Agronomie (IBiSA). High-throughput chromatin immunoprecipitation sequencing was performed at the Transriptomic and Genomic Marseille Luminy platform, supported by grants from Inserm, GIS IBiSA, Aix-Marseille Université, and ANR-10-INBS-0009-10.

Author affiliations: [a]BIAM, UMR 7265, Aix Marseille Univ, CEA, CNRS, Marseille, F-13009 France; [b]UMR CNRS 7267, Laboratoire Ecologie et Biologie des Interactions, Université de Poitiers, Poitiers, France; [c]Département de Biologie, Ecole Normale Supérieure, CNRS, Paris Sciences and Letters Research University, F-75005 Paris, France; [d]Université Paris-Sud, Université Paris-Saclay, 91405 Orsay, France; [e]Center for Sustainable Resource Science, RIKEN, Yokohama, 230-0045, Japan; [f]Institute of Plant Sciences Paris Saclay (IPS2), Université Paris-Saclay, CNRS, INRAE, Univ Evry, Orsay, 91405 France; and [g]IPS2, Université Paris Cité, CNRS, INRAE, Orsay, 91405 France

1. J. Wang, S. T. Lawry, A. L. Cohen, S. Jia, Chromosome boundary elements and regulation of heterochromatin spreading. *Cell. Mol. Life Sci.* **71**, 4841–4852 (2014).
2. H. J. Muller, Types of visible variations induced by X-rays in *Drosophila*. *J. Genet.* **22**, 299–334 (1930).
3. T. Ali, R. Renkawitz, M. Bartkuhn, Insulators and domains of gene expression. *Curr. Opin. Genet. Dev.* **37**, 17–26 (2016).
4. W. A. Bickmore, B. van Steensel, Genome architecture: Domain organization of interphase chromosomes. *Cell* **152**, 1270–1284 (2013).

5. J. Dekker, T. Misteli, Long-range chromatin interactions. *Cold Spring Harb. Perspect. Biol.* **7**, a019356 (2015).
6. J. R. Dixon *et al.*, Topological domains in mammalian genomes identified by analysis of chromatin interactions. *Nature* **485**, 376–380 (2012).
7. B. Bonev, G. Cavalli, Organization and function of the 3D genome. *Nat. Rev. Genet.* **17**, 772–772 (2016).
8. P. Heger, B. Marin, M. Bartkuhn, E. Schierenberg, T. Wiehe, The chromatin insulator CTCF and the emergence of metazoan diversity. *Proc. Natl. Acad. Sci. U.S.A.* **109**, 17507–17512 (2012).
9. C. Wang *et al.*, Genome-wide analysis of local chromatin packing in *Arabidopsis thaliana*. *Genome Res.* **25**, 246–256 (2015).
10. S. D. Singer, J. M. Hily, K. D. Cox, Analysis of the enhancer-blocking function of the TBS element from *Petunia hybrida* in transgenic *Arabidopsis thaliana* and *Nicotiana tabacum*. *Plant Cell Rep.* **30**, 2013–2025 (2011).
11. C. Liu, Y.-J. Cheng, J.-W. Wang, D. Weigel, Prominent topologically associated domains differentiate global chromatin packing in rice from *Arabidopsis*. *Nat. Plants* **3**, 742–748 (2017).
12. C. Liu, D. Weigel, Chromatin in 3D: Progress and prospects for plants. *Genome Biol.* **16**, 170 (2015).
13. J. Sequeira-Mendes, C. Gutierrez, Genome architecture: From linear organisation of chromatin to the 3D assembly in the nucleus. *Chromosoma* **125**, 455–469 (2016).
14. S. Grob, M. W. Schmid, N. W. Luedtke, T. Wicker, U. Grossniklaus, Characterization of chromosomal architecture in *Arabidopsis* by chromosome conformation capture. *Genome Biol.* **14**, R129 (2013).
15. S. Grob, M. W. Schmid, U. Grossniklaus, Hi-C analysis in *Arabidopsis* identifies the KNOT, a structure with similarities to the flamenco locus of *Drosophila*. *Mol. Cell* **55**, 678–693 (2014).
16. S. Feng *et al.*, Genome-wide Hi-C analyses in wild-type and mutants reveal high-resolution chromatin interactions in *Arabidopsis*. *Mol. Cell* **55**, 694–707 (2014).
17. A. Veluchamy *et al.*, LHP1 regulates H3K27me3 spreading and shapes the three-dimensional conformation of the *Arabidopsis* genome. *PLoS One* **11**, e0158936 (2016).
18. C. Liu *et al.*, Genome-wide analysis of chromatin packing in *Arabidopsis thaliana* at single-gene resolution. *Genome Res.* **26**, 1057–1068 (2016).
19. P. Fransz, H. de Jong, From nucleosome to chromosome: A dynamic organization of genetic information. *Plant J.* **66**, 4–17 (2011).
20. L. Simon, M. Voisin, C. Tatout, A. V. Probst, Structure and function of centromeric and pericentromeric heterochromatin in *Arabidopsis thaliana*. *Front. Plant Sci.* **6**, 1049 (2015).
21. S. Del Prete, J. Arpón, K. Sakai, P. Andrey, V. Gaudin, Nuclear architecture and chromatin dynamics in interphase nuclei of *Arabidopsis thaliana*. *Cytogenet. Genome Res.* **143**, 28–50 (2014).
22. P. Fransz, J. H. De Jong, M. Lysak, M. R. Castiglione, I. Schubert, Interphase chromosomes in *Arabidopsis* are organized as well defined chromocenters from which euchromatin loops emanate. *Proc. Natl. Acad. Sci. U.S.A.* **99**, 14584–14589 (2002).
23. W. J. J. Soppe *et al.*, DNA methylation controls histone H3 lysine 9 methylation and heterochromatin assembly in *Arabidopsis*. *EMBO J.* **21**, 6549–6559 (2002).
24. O. Mathieu, A. V. Probst, J. Paszkowski, Distinct regulation of histone H3 methylation at lysines 27 and 9 by CpG methylation in *Arabidopsis*. *EMBO J.* **24**, 2783–2791 (2005).
25. Z. Lippman *et al.*, Role of transposable elements in heterochromatin and epigenetic control. *Nature* **430**, 471–476 (2004).
26. Z. Vergara, C. Gutierrez, Emerging roles of chromatin in the maintenance of genome organization and function in plants. *Genome Biol.* **18**, 96 (2017).
27. A. Bergerat, D. Gadelle, P. Forterre, Purification of a DNA topoisomerase II from the hyperthermophilic archaeon Sulfolobus shibatae. A thermostable enzyme with both bacterial and eucaryal features. *J. Biol. Chem.* **269**, 27663–27669 (1994).
28. A. Bergerat *et al.*, An atypical topoisomerase II from Archaea with implications for meiotic recombination. *Nature* **386**, 414–417 (1997).
29. K. Schneider *et al.*, The ROOT HAIRLESS 1 gene encodes a nuclear protein required for root hair initiation in *Arabidopsis*. *Genes Dev.* **12**, 2013–2021 (1998).
30. K. Schneider, B. Wells, L. Dolan, K. Roberts, Structural and genetic analysis of epidermal cell differentiation in *Arabidopsis* primary roots. *Development* **124**, 1789–1798 (1997).
31. K. Sugimoto-Shirasu *et al.*, RHL1 is an essential component of the plant DNA topoisomerase VI complex and is required for ploidy-dependent cell growth. *Proc. Natl. Acad. Sci. U.S.A.* **102**, 18736–18741 (2005).
32. H. J. Yoon *et al.*, *Lotus japonicus* SUNERGOS1 encodes a predicted subunit A of a DNA topoisomerase VI that is required for nodule differentiation and accommodation of rhizobial infection. *Plant J.* **78**, 811–821 (2014).
33. F. Hartung, H. Puchta, Molecular characterization of homologues of both subunits A (SPO11) and B of the archaebacterial topoisomerase 6 in plants. *Gene* **271**, 81–86 (2001).
34. F. Hartung *et al.*, An archaebacterial topoisomerase homolog not present in other eukaryotes is indispensable for cell proliferation of plants. *Curr. Biol.* **12**, 1787–1791 (2002).
35. Y. Yin *et al.*, A crucial role for the putative *Arabidopsis* topoisomerase VI in plant growth and development. *Proc. Natl. Acad. Sci. U.S.A.* **99**, 10191–10196 (2002).
36. A. Mittal *et al.*, TOPOISOMERASE 6B is involved in chromatin remodelling associated with control of carbon partitioning into secondary metabolites and cell walls, and epidermal morphogenesis in *Arabidopsis*. *J. Exp. Bot.* **65**, 4217–4239 (2014).
37. K. Sugimoto-Shirasu, N. J. Stacey, J. Corsar, K. Roberts, M. C. McCann, DNA topoisomerase VI is essential for endoreduplication in *Arabidopsis*. *Curr. Biol.* **12**, 1782–1786 (2002).
38. C. Breuer *et al.*, BIN4, a novel component of the plant DNA topoisomerase VI complex, is required for endoreduplication in *Arabidopsis*. *Plant Cell* **19**, 3655–3668 (2007).
39. V. Kirik, A. Schrader, J. F. Uhrig, M. Hulskamp, MIDGET unravels functions of the *Arabidopsis* topoisomerase VI complex in DNA endoreduplication, chromatin condensation, and transcriptional silencing. *Plant Cell* **19**, 3100–3110 (2007).
40. E. L. Meczes, K. L. Gilroy, K. L. West, C. A. Austin, The impact of the human DNA topoisomerase II C-terminal domain on activity. *PLoS One* **3**, e1754 (2008).
41. A. Onoda *et al.*, Nuclear dynamics of topoisomerase IIβ reflects its catalytic activity that is regulated by binding of RNA to the C-terminal domain. *Nucleic Acids Res.* **42**, 9005–9020 (2014).
42. K. L. Gilroy, C. A. Austin, The impact of the C-terminal domain on the interaction of human DNA topoisomerase II α and β with DNA. *PLoS One* **6**, e14693 (2011).
43. Y. Pommier, Y. Sun, S. N. Huang, J. L. Nitiss, Roles of eukaryotic topoisomerases in transcription, replication and genomic stability. *Nat. Rev. Mol. Cell Biol.* **17**, 703–721 (2016).
44. M. Jain, A. K. Tyagi, J. P. Khurana, Overexpression of putative topoisomerase 6 genes from rice confers stress tolerance in transgenic *Arabidopsis* plants. *FEBS J.* **273**, 5245–5260 (2006).
45. M. Jain, A. K. Tyagi, J. P. Khurana, Constitutive expression of a meiotic recombination protein gene homolog, OsTOP6A1, from rice confers abiotic stress tolerance in transgenic *Arabidopsis* plants. *Plant Cell Rep.* **27**, 767–778 (2008).
46. K. Simková *et al.*, Integration of stress-related and reactive oxygen species-mediated signals by Topoisomerase VI in *Arabidopsis thaliana*. *Proc. Natl. Acad. Sci. U.S.A.* **109**, 16360–16365 (2012).
47. C. J. Underwood, I. R. Henderson, R. A. Martienssen, Genetic and epigenetic variation of transposable elements in *Arabidopsis*. *Curr. Opin. Plant Biol.* **36**, 135–141 (2017).
48. K. De Preter, R. Barriot, F. Speleman, J. Vandesompele, Y. Moreau, Positional gene enrichment analysis of gene sets for high-resolution identification of overrepresented chromosomal regions. *Nucleic Acids Res.* **36**, e43 (2008).
49. J. Sequeira-Mendes *et al.*, The functional topography of the *Arabidopsis* genome is organized in a reduced number of linear motifs of chromatin states. *Plant Cell* **26**, 2351–2366 (2014).
50. L. Shen *et al.*, diffReps: Detecting differential chromatin modification sites from ChIP-seq data with biological replicates. *PLoS One* **8**, e65598 (2013).
51. H. Stroud *et al.*, Non-CG methylation patterns shape the epigenetic landscape in *Arabidopsis*. *Nat. Struct. Mol. Biol.* **21**, 64–72 (2014).
52. P. Zhang *et al.*, MetaCyc and AraCyc. Metabolic pathway databases for plant research. *Plant Physiol.* **138**, 27–37 (2005).
53. Y. Chen, T. Zou, S. McCormick, S-adenosylmethionine synthetase 3 is important for pollen tube growth. *Plant Physiol.* **172**, 244–253 (2016).
54. F. Roudier *et al.*, Integrative epigenomic mapping defines four main chromatin states in *Arabidopsis*. *EMBO J.* **30**, 1928–1938 (2011).
55. I. Ahmed, A. Sarazin, C. Bowler, V. Colot, H. Quesneville, Genome-wide evidence for local DNA methylation spreading from small RNA-targeted sequences in *Arabidopsis*. *Nucleic Acids Res.* **39**, 6919–6931 (2011).
56. S. R. Eichten *et al.*, Spreading of heterochromatin is limited to specific families of maize retrotransposons. *PLoS Genet.* **8**, e1003127 (2012).
57. Z. Lang *et al.*, The methyl-CpG-binding protein MBD7 facilitates active DNA demethylation to limit DNA hyper-methylation and transcriptional gene silencing. *Mol. Cell* **57**, 971–983 (2015).
58. H. Saze, A. Shiraishi, A. Miura, T. Kakutani, Control of genic DNA methylation by a jmjC domain-containing protein in *Arabidopsis thaliana*. *Science (80-.).* **319**, 462–465 (2008).
59. H. Jiang *et al.*, Ectopic application of the repressive histone modification H3K9me2 establishes post-zygotic reproductive isolation in *Arabidopsis thaliana*. *Genes Dev.* **31**, 1272–1287 (2017).
60. J. M. Wendte *et al.*, Epimutations are associated with CHROMOMETHYLASE 3-induced de novo DNA methylation. *eLife* **8**, e47891 (2019).
61. S. Inagaki *et al.*, Gene-body chromatin modification dynamics mediate epigenome differentiation in *Arabidopsis*. *EMBO J.* **36**, 970–980 (2017).
62. R. Stunnenberg *et al.*, H3K9 methylation extends across natural boundaries of heterochromatin in the absence of an HP1 protein. *EMBO J.* **34**, 2789–2803 (2015).
63. K. Jamieson *et al.*, Loss of HP1 causes depletion of H3K27me3 from facultative heterochromatin and gain of H3K27me2 at constitutive heterochromatin. *Genome Res.* **26**, 97–107 (2016).
64. Y. Lu, G. Shan, J. Xue, C. Chen, C. Zhang, Defining the multivalent functions of CTCF from chromatin state and three-dimensional chromatin interactions. *Nucleic Acids Res.* **44**, 6200–6212 (2016).
65. S. He, M. Vickers, J. Zhang, X. Feng, Natural depletion of histone H1 in sex cells causes DNA demethylation, heterochromatin decondensation and transposon activation. *eLife* **8**, e42530 (2019).
66. G. Moissiard *et al.*, MORC family ATPases required for heterochromatin condensation and gene silencing. *Science* **336**, 1448–1451 (2012).
67. Z. J. Lorković, U. Naumann, A. J. M. Matzke, M. Matzke, Involvement of a GHKL ATPase in RNA-directed DNA methylation in *Arabidopsis thaliana*. *Curr. Biol.* **22**, 933–938 (2012).
68. T. R. Brabbs *et al.*, The stochastic silencing phenotype of Arabidopsis morc6 mutants reveals a role in efficient RNA-directed DNA methylation. *Plant J.* **75**, 836–846 (2013).
69. M. Witcher, B. M. Emerson, Epigenetic silencing of the p16(INK4a) tumor suppressor is associated with loss of CTCF binding and a chromatin boundary. *Mol. Cell* **34**, 271–284 (2009).
70. T. M. Yusufzai, H. Tagami, Y. Nakatani, G. Felsenfeld, CTCF tethers an insulator to subnuclear sites, suggesting shared insulator mechanisms across species. *Mol. Cell* **13**, 291–298 (2004).
71. L. Uusküla-Reimand *et al.*, Topoisomerase II beta interacts with cohesin and CTCF at topological domain borders. *Genome Biol.* **17**, 182 (2016).
72. M. Manohar *et al.*, Plant and human MORC proteins have DNA modifying activities similar to type II topoisomerases, but require additional factor(s) for full activity. *Mol. Plant Microbe Interact.* **30**, 87–100 (2017).
73. J. Meng *et al.*, Methionine Adenosyltransferase4 mediates DNA and histone methylation. *Plant Physiol.* **177**, 652–670 (2018).
74. Y. Katoh *et al.*, Methionine adenosyltransferase II serves as a transcriptional corepressor of Maf oncoprotein. *Mol. Cell* **41**, 554–566 (2011).
75. Y. Kera *et al.*, Methionine adenosyltransferase II-dependent histone H3K9 methylation at the COX-2 gene locus. *J. Biol. Chem.* **288**, 13592–13601 (2013).
76. N. E.. Yelina *et al.*, Epigenetic remodeling of meiotic crossover frequency in *Arabidopsis thaliana* DNA methyltransferase mutants. *PLoS Genet.* **8**, e1002844 (2012).
77. H. Thorvaldsdóttir, J. T. Robinson, J. P. Mesirov, Integrative genomics viewer (IGV): High-performance genomics data visualization and exploration. *Brief. Bioinform.* **14**, 178–192 (2013).